sustainability

MDPI

Article

Numerical Modeling and Design Method for Reinforced Polyvinyl-Alcohol-Engineered Cementitious Composite Beams in Bending

Qiao-Ling Fu [1], Shao-Bo Kang [2] and Dan-Dan Wang [2,*]

[1] Faculty of Architectural Engineering, Chongqing Water Resources and Electric Engineering College, Chongqing 402171, China; ginkgoling@163.com
[2] School of Civil Engineering, Chongqing University, Chongqing 400044, China
* Correspondence: wangdd0914@cqu.edu.cn

Abstract: The polyvinyl-alcohol-engineered cementitious composite (PVA-ECC) is a superior cementitious material when used for tension and flexural loading. The utilization of PVA-ECC in the tension zone can prevent the development of wide cracks and increase the flexural resistance of reinforced PVA-ECC members. In this paper, a nonlinear finite element model is established to simulate the behavior of PVA-ECC beams in bending. In the model, the constitutive models for PVA-ECC in compression and tension are employed by simplifying them as piece-wise linear models, and the bond between the reinforcing bar and PVA-ECC is also considered. The load–deflection curve and failure mode of beams can be obtained from the finite element model. Comparisons between numerical and experimental results show that the developed numerical model can estimate the ultimate load and failure mode of beams with reasonably good accuracy. After evaluating the accuracy of the finite element model, parameter analysis is conducted to investigate the effects of the reinforcement ratio, steel strength grade, and mechanical properties of PVA-ECC on the flexural behavior of reinforced PVA-ECC beams. The numerical results conclude that the effects of reinforcement ratio on the peak load, stiffness, and deflection are obvious while the influence of steel grade is mainly on the peak load. The tensile localization strain of PVA-ECC mainly affects the ductility of the beam. Furthermore, a design method is proposed based on the plane-section assumption to calculate the ultimate load of reinforced PVA-ECC beams, in which the contribution of PVA-ECC to the moment resistance of beam sections is considered. Comparisons between existing design methods and the proposed method indicate that the ultimate load of beams can be predicted more accurately by considering the tensile strength of PVA-ECC in the tension zone.

Keywords: finite element analysis; bond–slip model; load–deflection relationship; failure mode; design method

Citation: Fu, Q.-L.; Kang, S.-B.; Wang, D.-D. Numerical Modeling and Design Method for Reinforced Polyvinyl-Alcohol-Engineered Cementitious Composite Beams in Bending. *Sustainability* **2023**, *15*, 10130. https://doi.org/10.3390/su151310130

Academic Editors: Mahdi Kioumarsi and Vagelis Plevris

Received: 2 June 2023
Revised: 19 June 2023
Accepted: 22 June 2023
Published: 26 June 2023

1. Introduction

The polyvinyl-alcohol-engineered cementitious composite (PVA-ECC) is a superior cementitious material for its excellent mechanical properties under tension. Combined with discontinuous fiber, the ECC can mitigate the development of major cracks and attain a tensile strain capacity higher than 3% [1–3]. As a bendable concrete suitable for sustainable and resilient infrastructure, ECC has been studied by many researchers and has been applied in high buildings, bridge structures, and high railways [4].

Due to its superior tensile properties, the application of ECC in the tension zone of flexural members has been investigated by many researchers [5]. Ge et al. [5] studied the effect of reinforcement type and ECC thickness on the flexural behavior of reinforced ECC-concrete beams. The moment capacity and bending stiffness were enhanced and the crack width was well controlled when ECC was used to replace the concrete with the same thickness. Yuan et al. [6] investigated the flexural behavior of

ECC/concrete composite beams and confirmed the enhancement from ECC to the flexural resistance of reinforced concrete beams. Apart from the application of ECC in the tension zone, flexural properties of the whole ECC beam have also aroused great interest. Even though the influence of concrete type and reinforcement ratio on reinforced concrete beams has been investigated [7–10], its effect on PVA-ECC beams showed different results. Shao et al. [11–13] proposed two failure paths of PVA-ECC beams, namely, failure after a dominant crack or after gradual strain hardening of a reinforcement, depending on the reinforcement ratio. According to the test results of twelve simply supported beams, the failure paths were mainly affected by the reinforcing ratio and steel type. A simplified flexural strength prediction method was also proposed to predict the load-bearing capacity of ECC beams. The shear behavior of reinforced ECC beams has also been investigated by researchers from different countries [14–16].

Besides experimental results, finite element simulations were also utilized to study the behavior of reinforced PVA-ECC beams. Zheng et al. [17] adopted ABAQUS/Standard software to estimate the shear capacity of RC beams strengthened by ECC composite layers. Shanour et al. [18] tested twelve reinforced ECC beams with different ratios of PVA and polypropylene fibers. Nonlinear element analysis was also conducted to predict the load–deflection curves and crack patterns of ECC beams. However, the calculated initial stiffness from the numerical results was greater than that from the experimental results. Selim et al. [19] developed three-dimensional finite element models for beams under four-point loading by using ABAQUS. The numerical results were in good agreement with the test results at the initial loading stage, followed by significant differences at the peak load. Shao et al. [20] adopted a new ECC compression model to simulate the gradual compression softening behavior of flexural members by using nonlinear element analysis software DIANA. The numerical results concluded that the proposed model with the new compression model and a hybrid-rotating/fixed-crack model predicts the beam behavior, especially the failure mode and drift capacity of beams, with good accuracy.

To predict the flexural properties of reinforced PVA-ECC beams, a nonlinear finite element model without initial flaws is proposed in this paper. Six four-point bending specimens from the literature [21] are simulated to evaluate the accuracy of the proposed model. Parameter analyses are conducted to investigate the effect of the reinforcement ratio, steel strength grade, and mechanical properties of PVA-ECC on the load–deflection behavior. In addition, a design method is developed to consider the tensile strength of PVA-ECC in calculating the moment capacity of beams. Comparisons are made between different design methods and test data to show the effect of the tensile strength of PVA-ECC in beams.

2. Numerical Model

2.1. Finite Element Models

In reference [11], singly reinforced PVA-ECC beams were tested in four-point bending. The PVA-ECC used for beams was designed by using cement, fly ash, sand, PVA fibers, and superplasticizer. Cement, fly ash, and sand were put into a mixer and mixed for about five minutes, and then fibers were put in the cement paste and mixed for three minutes to ensure uniform dispersions. Nonlinear finite element analysis is conducted to model the flexural behavior of the PVA-ECC beam. Software DIANA FEA [22] is employed to simulate the load–deflection curves and failure modes of the beam. Figure 1 shows the geometry, test setup, and finite element model for the beam. A two-dimensional model with a quadrilateral mesh is used for the beam. Simple supports are defined at the two ends of the beams. The plane stress element is defined for PVA-ECC and the mesh size is 10 mm $\times$ 10 mm with a 150 mm thickness. The height of the cross-section is 250 mm. Stirrup and longitudinal reinforcements are embedded into the PVA-ECC. As for longitudinal reinforcements, the bond–slip behavior between PVA-ECC and the reinforcement is taken into consideration. A displacement-control load is applied at the middle point of steel block, with 0.1 mm at each step in the simulation.

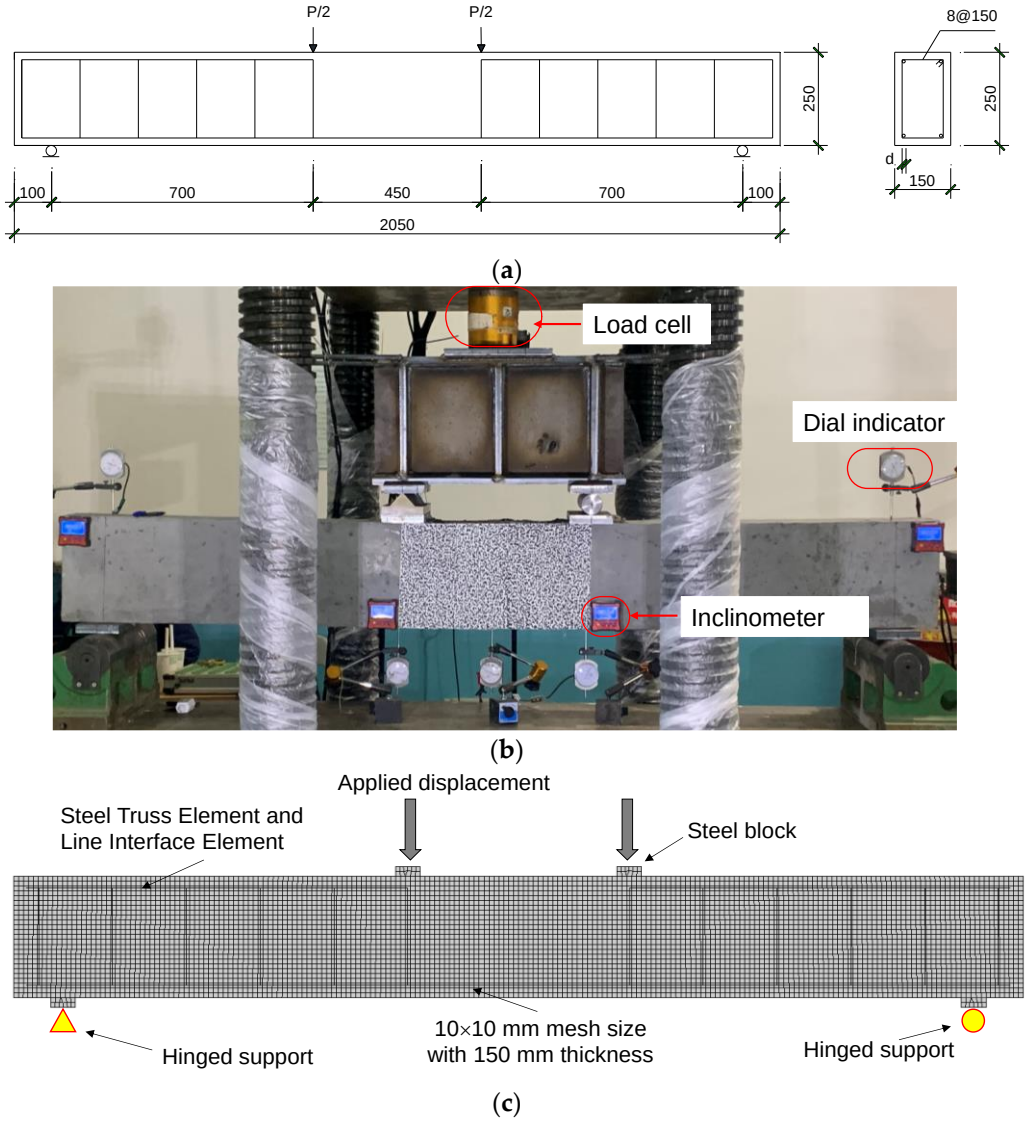

Figure 1. Finite element model for simply supported beams. (**a**) Geometry of beams. (**b**) Experimental setup. (**c**) Finite element model.

The mechanical model of PVA-ECC used in the simulations is based on tension and compression tests conducted by Shao [12]. As shown in Figure 2a, four stages are observed from the compressive stress–strain curve, namely, the elastic stage, nonlinear riding stage, linear descending stage, and plateau stage. Table 1 summarizes the mechanical properties of PVA-ECC in tension and compression. In the table, f_r represents the residual compressive stress and is suggested to be 30% of the peak stress in this paper, $\varepsilon_{c,p}$ represents the peak strain when the compressive strength is reached, $\varepsilon_{c,1/2}$ is obtained using a compressive stress equal to 0.5 times the peak stress divided by the elastic modulus, and $\varepsilon_{c,u}$ is the residual strain when the residual stress reaches 30% of the peak stress.

The constitutive model for ECC in tension is simplified as four stages, namely, the elastic stage (OA), linear rising stage (AB), plateau stage (BC), and linear softening stage (BC), as shown in Figure 2b. Table 1 shows values of tensile stress and strain at different stages in the numerical simulation. In the table, f_t is taken as 1.96 MPa according to four-point flexural tests; $f_{t,cr}$ represents the tensile cracking strength and is recommended to be 1.86 MPa; $f_{t,cr}$ is assumed to be 95% of the tensile strength f_t [20]; $\varepsilon_{t,cr}$ represents the tensile strain when the stress is 0.95 times the peak strain; $\varepsilon_{t,1}$ is the tensile cracking strain when obvious cracking forms; $\varepsilon_{t,p}$ is the tensile strain when a principal crack forms, namely, the

localization strain. The steel constitutive model adopts the elastoplastic model and detailed data are shown in the literature [21].

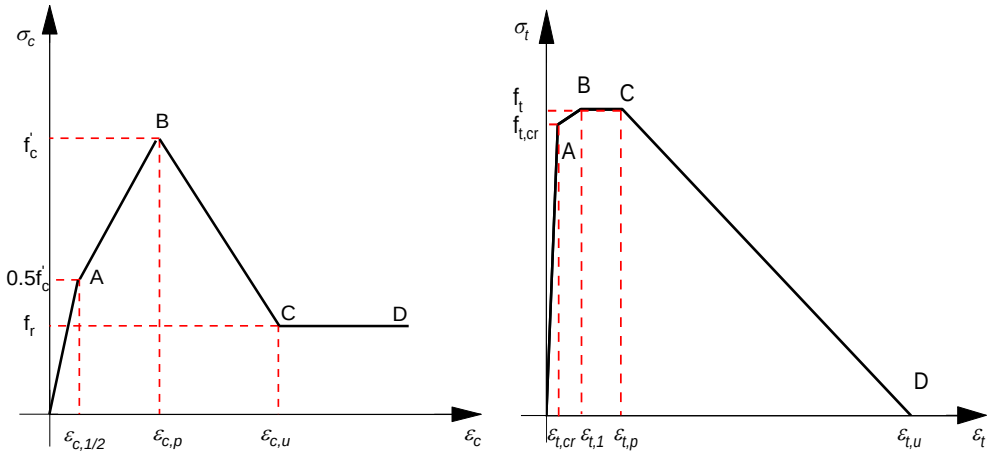

Figure 2. Mechanical properties of PVC-ECC: (**a**) compressive constitutive model; (**b**) tensile constitutive model.

Table 1. ECC properties in numerical model.

Parameter	Symbol	Unit	ECC
Compressive strength	f_c'	MPa	38.5
Compressive strain at peak strength	$\varepsilon_{c,p}$	mm/mm	0.0034
Compressive strain at 0.5 times the peak strength	$\varepsilon_{c,1/2}$	mm/mm	0.0011
Compressive strain at the residual strain	$\varepsilon_{c,u}$	mm/mm	0.005
Elastic modulus	E_c	GPa	17.1
Tensile strength	f_t	MPa	1.96
Tensile cracking strength	$f_{t,cr}$	MPa	1.86
Tensile strain when the stress is 0.95 times of peak stress	$\varepsilon_{t,cr}$	mm/mm	0.00011
Tensile cracking strain	$\varepsilon_{t,1}$	mm/mm	0.0011
Tensile localization strain	$\varepsilon_{t,p}$	mm/mm	0.0073
Maximum tensile strain of ECC	$\varepsilon_{t,u}$	mm/mm	0.035

The longitudinal reinforcement is embedded in PVA-ECC. The embedded reinforcement element coupled with concrete elements deforms together as a whole and contributes to the stiffness. In DIANA software, the bond–slip model of the reinforcement can be defined based on the embedded reinforcement element without the definition of an interface element, which can save time and improve modeling efficiency. The bond–slip relationship between ECC and the reinforcement is shown in Figure 3. Equation (1) shows the equation of the bond–slip curve proposed by Shao et al. [20] and Bandelt et al. [23]. The bond–slip curve consists of three stages, including a nonlinear ascending stage, a linear descending stage, and a plateau stage resulting from the presence of a frictional bond.

$$\frac{\tau}{1.17 \cdot \tau_{\max}} = \begin{cases} s^{0.28} & s \le s_1 \\ 1 - 0.06 \cdot (s-1) & s_1 < s \le s_2 \\ 0.3 & s_2 < s \end{cases} \quad (1)$$

where $\tau_{\max}$ is the peak bond stress and can be taken as $1.2\sqrt{f_c'}$; s_1 and s_2 are quantified to be 1 and 12.7, respectively.

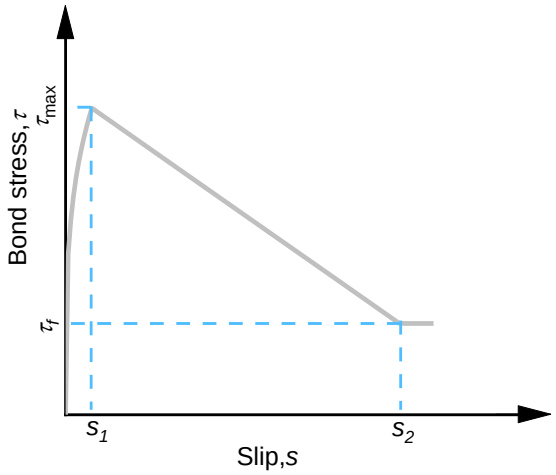

Figure 3. Bond–slip model between ECC and steel bars.

2.2. Validation of Proposed Model

Before simulations, a mesh sensitivity is performed to calibrate the finite element model with different mesh sizes for specimen ECC-16-1.072, namely, 25 mm, 10 mm, and 5 mm. It can be seen from Figure 4 that the load–deflection curves are identical to each other for three mesh sizes before peak load is reached. However, the load–deflection relationship after the peak load is lower than that of the experimental results when the mesh size is increased to 25 mm. Even though the results with a mesh size of 5 mm are closer to the test result, the simulation is time-consuming, taking more than 24 h, which is not appropriate. Therefore, a mesh size of 10 mm is suitable for numerical modeling.

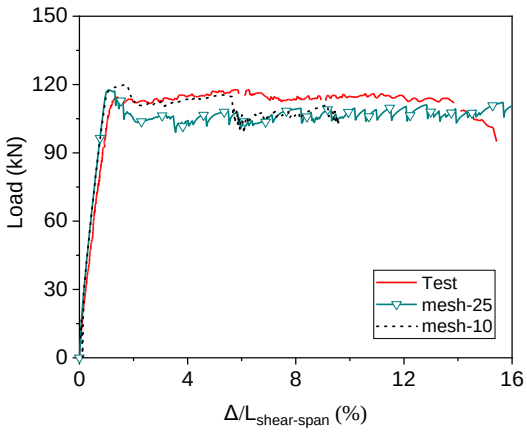

Figure 4. Parameter analysis on mesh size for specimen ECC-16–1.072.

Figure 5 compares the load–deflection curves of three PVA-ECC beams obtained in the experimental tests and numerical models. Note that the blue cross denotes the point where the fracture of rebars occurs. It can be observed from the figure that the load–deflection curves of the numerical results are in good agreement with the experiment results at the initial and ultimate stages. The maximum load capacity of experimental and numerical results is shown in Table 2. The ratio of numerical results to experimental results of the peak load ranges between 1.01 and 1.07, with a mean value of 1.04. The mean ratio of the beam deflection at the fracture of rebars is 0.96, with a coefficient of variation of 6.7%, as shown in Table 2. It indicates that the ultimate load of beams is slightly overestimated by using the developed numerical model, whereas the deflection at the fracture of reinforcement is underestimated. The overestimation of the load capacity might come from the difference between the actual and measured tensile strengths of PVA-ECC. In reinforced PVA-ECC beams, the presence of flaws in PVA-ECC can reduce its tensile strength.

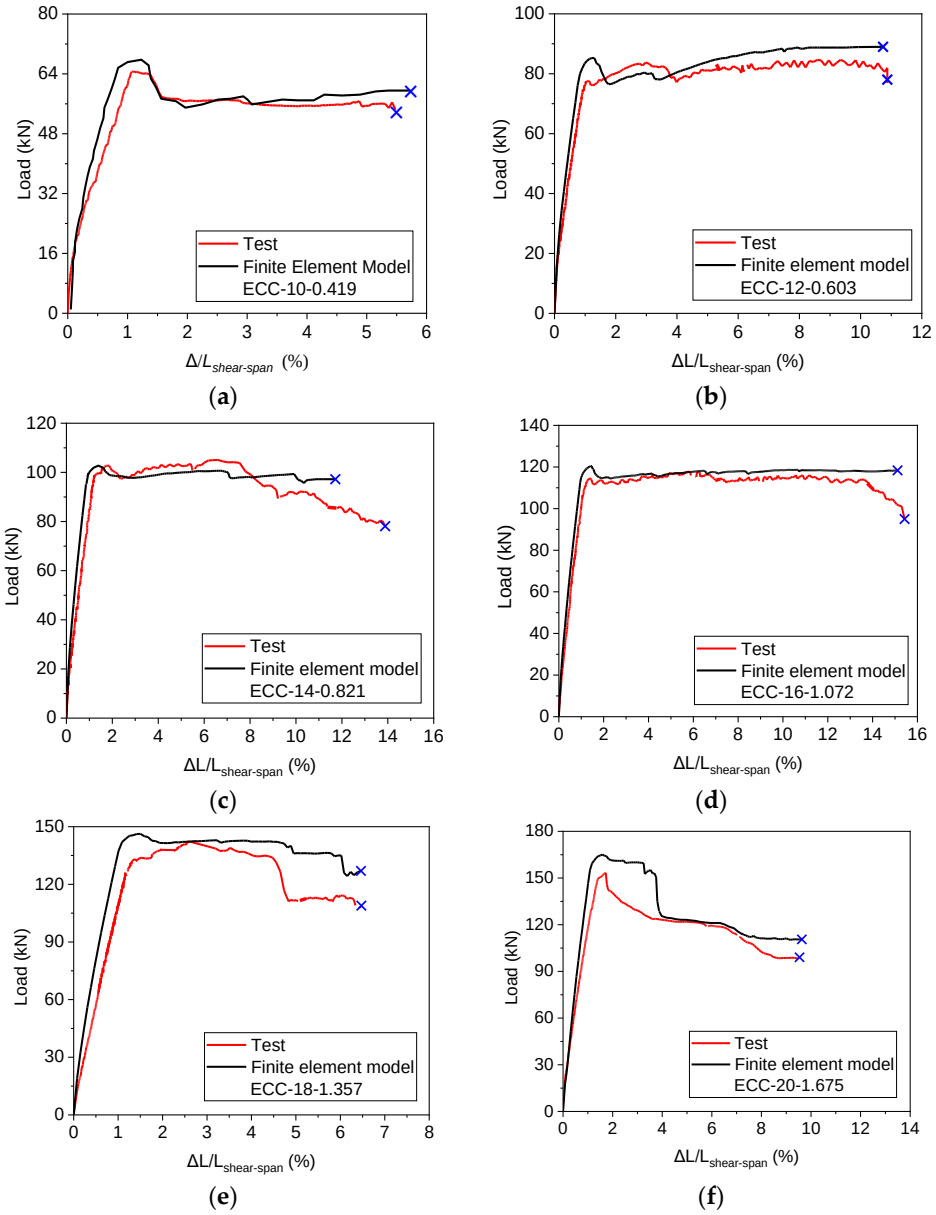

Figure 5. Experimental and numerical results of load deflection curves: (**a**) ECC-10-0.419; (**b**) ECC-12-0.603; (**c**) ECC-14-0.821; (**d**) ECC-14-0.821; (**e**) ECC-14-0.821; (**f**) ECC-14-0.821.

Figure 6 shows the principal tensile strain contours of the three specimens. Similar to the experimental results, the failure model of ECC-10–0.419 is due to the fracture of reinforcement in the tension zone, as shown in Figure 6a, and then the load value decreases sharply. When the reinforcement ratio is increased to 1.075% (see Figure 6b) and 1.675% (see Figure 6c), the purple zone, namely, the compression zone, is extended and the crack length across the section decreases. This indicates that the failure model is changed from the fracture of steel reinforcement to the crushing of the compression zone. Thus, the failure mode of reinforced PVA-ECC beams depends highly on the reinforcement ratio at the bottom side. When the reinforcement ratio is low, fracture of the tensile reinforcement occurs near the loading points, leading to the failure of beams. However, if the reinforcement is high, crushing of PVA-ECC may occur in the compression zone first, resulting in significant reductions in the applied load.

Besides the principle tensile strain, the strain of steel reinforcement can also be obtained from the numerical model. The maximum stress of the beam bottom reinforcement is located at the midspan of beams, with a value of 509.0 MPa for specimen ECC-10-0.419.

With the increase in reinforcement ratio, the maximum steel stress decreases from 509.0 MPa to 463.4 MPa. With regard to the top reinforcement, the compression stress increases from 35.8 MPa to 125.5 MPa when the reinforcement ratio increases from 0.419% to 1.675%.

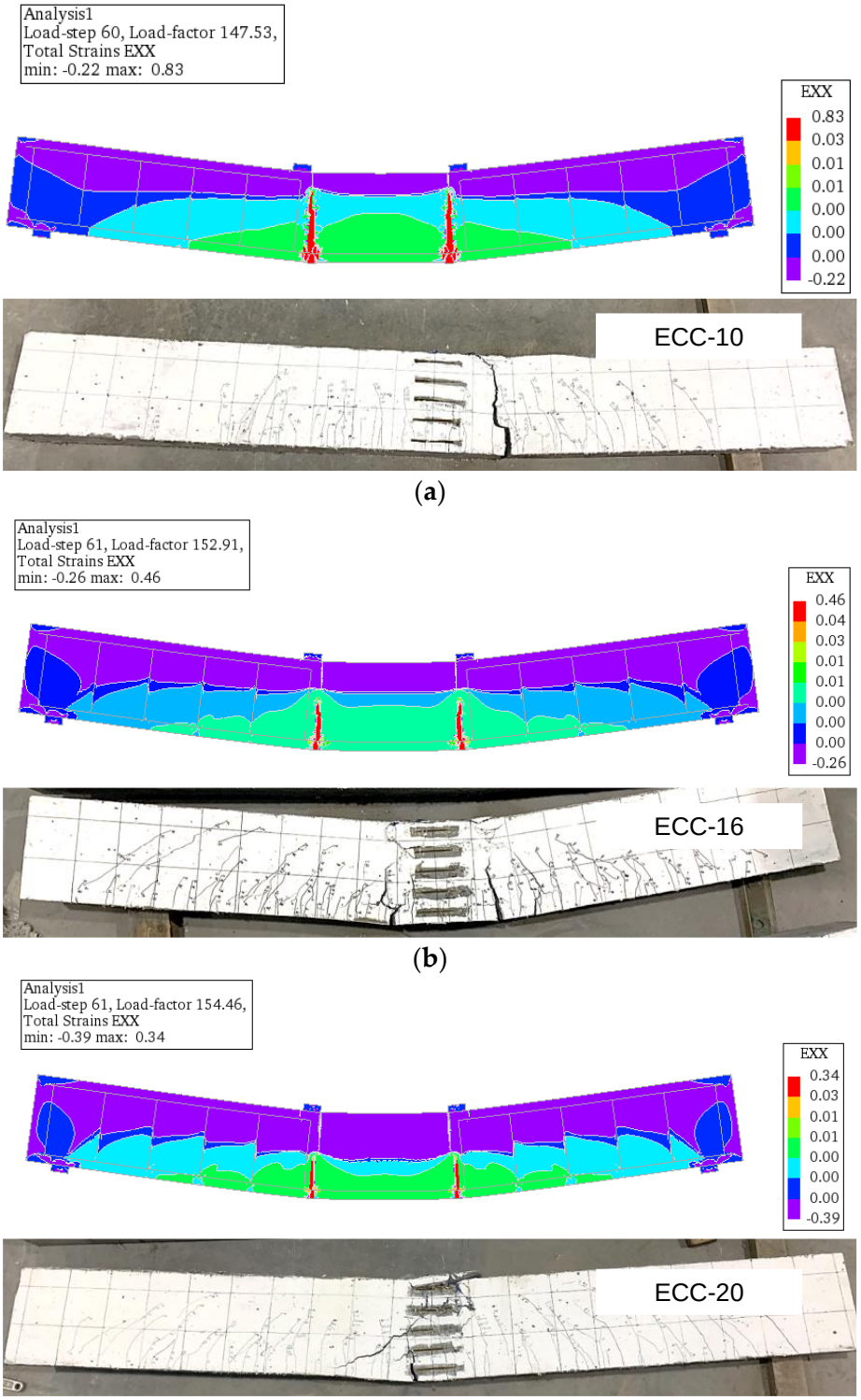

Figure 6. Principal tensile strains of beams in bending: (**a**) ECC-10-0.419; (**b**) ECC-16-1.075; (**c**) ECC-20-1.675.

Table 2. Comparison of test results and finite element results.

Specimen	Ultimate Load			Deflection at Fracture of Rebars		
	Experimental Results P_{Exp} (kN)	Numerical Results P_{FE} (kN)	P_{FE}/P_{Exp}	Experimental Results D_{Exp} (%)	Numerical Results D_{FE} (%)	D_{FE}/D_{Exp}
ECC-10-0.419	64.7	68.2	1.05	5.94	5.97	1.01
ECC-12-0.603	84.7	88.7	1.05	10.99	10.34	0.94
ECC-14-0.821	102.8	103.5	1.01	13.91	11.71	0.84
ECC-16-1.072	117.7	120.5	1.02	15.55	15.11	0.97
ECC-18-1.357	142.4	146.3	1.03	6.62	6.46	0.98
ECC-20-1.675	153.4	164.3	1.07	9.53	9.63	1.01
Average			1.04			0.96
Coefficient of variation			2.2%			6.7%

2.3. Parameter Analysis

With the verified numerical model, three beams with different reinforcement ratios of 0.269%, 0.343%, and 0.419% are modeled to study the effect of reinforcement ratio on the flexural behavior of beams. Other parameters of the beam remain the same as those of ECC-10-0.419. Figure 7a shows the load–deflection curves with different reinforcement ratios. It can be observed that specimen ECC-10-0.419 develops the highest load after the development of a principal crack. The effects of reinforcement ratio on the peak load, stiffness, and deflection are obvious when the specimen fails. By reducing the reinforcement ratio from 0.419% to 0.269%, the ultimate load of the beam is considerably decreased. The initial stiffness of beams is nearly the same before the cracking of PVA-ECC, whereas the stiffness after the cracking of PVA-ECC shows a remarkable difference due to the development of microcracks. The stiffness following the cracking of PVA-ECC decreases gradually with decreasing reinforcement ratio.

In addition to the reinforcement ratio, the influence of steel grade, maximum tensile strain, tensile localization strain, and bond strength on the flexural behavior of beams is also investigated using the numerical model. Three different steel grades, namely, yield strengths of 335 MPa, 450 MPa, and 500 MPa, are selected in the numerical simulation. Figure 7b presents the load–deflection relationship of beams with different steel strengths. The peak loads of the three specimens are 54.7 kN, 64.3 kN, and 68.4 kN for beams with steel yield strengths of 335 MPa, 450 MPa, and 500 MPa, respectively. This indicates that the ultimate of beams can be enhanced if the reinforcement strength increases. As for the deformation capacity, namely, the deflection at which the load decreases to 85% of the ultimate load, it is increased slightly with increasing steel yield strength, as shown in Figure 7b. The influences of the maximum tensile strain and tensile localization strain on load–deflection curves are also discussed, as shown in Figure 7c,d. It can be seen from these three figures that the ultimate tensile strain of ECC does not have a significant effect on the load–deflection curve of beams when the value varies between 0.001 and 0.035. Nevertheless, when the tensile localization strain varies from 0.005 and 0.010, the deformation capacity of beams is considerably increased, but the ultimate load of beams is not considerably affected.

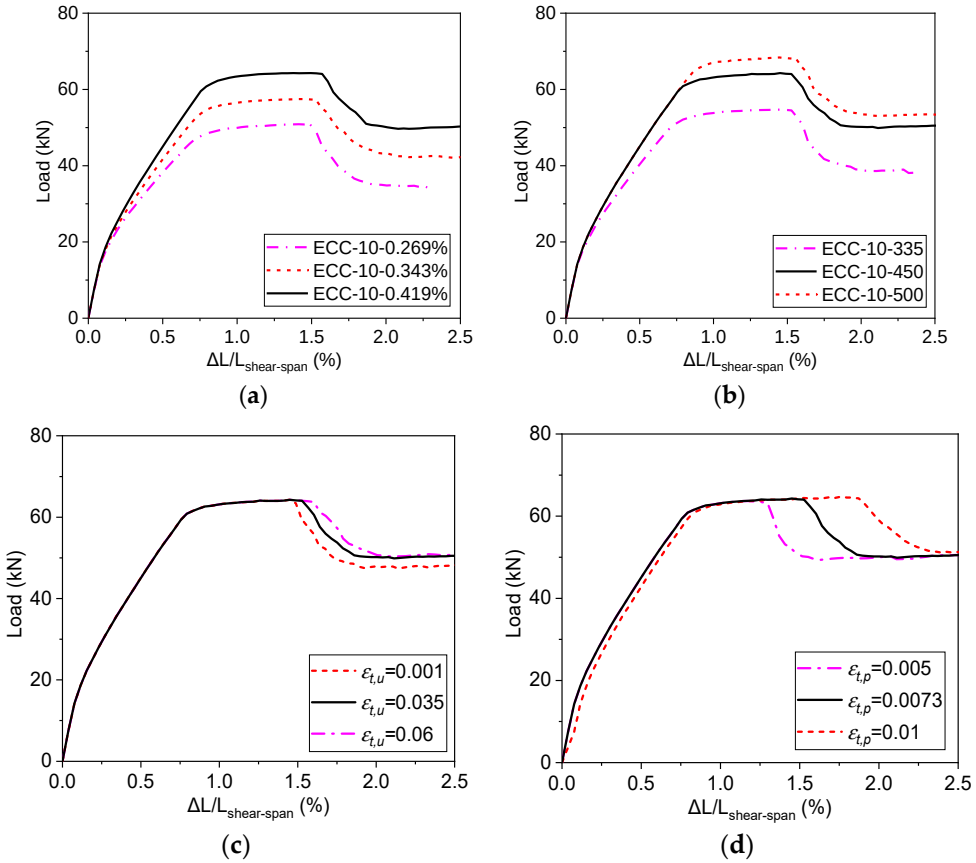

Figure 7. Load–deflection curve of test beam with different reinforcement ratios and steel bar strengths: (**a**) reinforcement ratio; (**b**) steel bar strength; (**c**) maximum tensile strain; (**d**) tensile localization strain.

3. Existing Design Methods

Numerical modeling is used to predict the load–deflection curves, crack width of singly reinforced beams. Even though it is possible to obtain multiple simulation results, the calculation procedure is time-consuming and complicated. To obtain the peak load easily and concisely, existing design methods are used to calculate the ultimate load of reinforced PVA-ECC beams and are then compared with test data to show their accuracy.

3.1. American Concrete Institute and Chinese Code

For conventional concrete beams, American concrete institution and Chinese guidelines propose similar calculation methods for the load-bearing capacity based on the plane-section assumption. They assume that the maximum strain at the extreme concrete compression fiber is equal to 0.003 and the tensile strength of concrete is neglected. The compressive stress in the compression zone is represented by a rectangular compressive stress block. Equations (2) and (3) show the calculation method of moment capacity. Table 3 shows the peak load of reinforced PVA-ECC beams calculated by using GB 50010-2010 [24] and ACI 318-19 [25]. For the design method in GB 50010-2010, it cannot consider the contribution of PVA fibers. However, for reinforced PVA-ECC beams, the tensile strength of PVA-ECC has not been exhausted when the load capacity of the beam is reached. As a result, the peak load is far lower than the experimental values except for specimen ECC-20-1.675. Hence, the tensile strength of PVA-ECC has to be considered. The peak load of all specimens calculated by ACI-318-19 is also lower than the experiment result. Therefore, it

is essential to consider the contribution of fibers in the tension zone while calculating the peak load of PVA-ECC beams.

$$M = \alpha_1 \beta_b f_c b x (h_0 - x/2) \tag{2}$$

$$x = \frac{f_y A_s}{\alpha_1 \beta_b f_c b} \tag{3}$$

where β_b represents the simplified coefficient and is 0.85 and 0.8 in ACI-318-19 [25] and GB 50010-2010 [24], respectively.

3.2. *fib Model Code*

fib Model Code [26] proposes a calculation method to consider the influence of fiber in the tension zone. Flexural failure occurs when one of the following conditions is reached (see Figure 8):

1. Attainment of the ultimate compressive strain of ECC, $\varepsilon_{c,u}$;
2. Attainment of the ultimate tensile stain in the steel, $\varepsilon_{s,u}$;
3. Attainment of the ultimate tensile strain of ECC, $\varepsilon_{t,u}$'

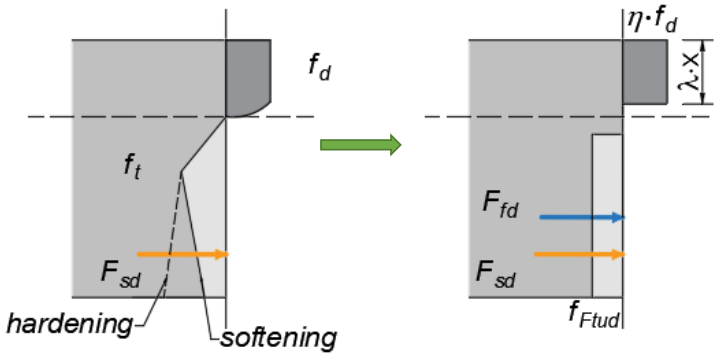

Figure 8. Calculation of bending moment from *fib Model Code*.

Similar to conventional concrete, it is assumed that the ultimate compressive strain of ECC is achieved. In order to calculate the compressive stress and tensive stress conveniently, a rectangular zone is used in the compression and tension zones, as shown in Figure 8. The second condition is neglected in the calculation, as the steel bar is at the post-yield stage when PVA-ECC beams achieve the peak load. Coefficients λ and η adopt 0.8 and 1.0 from *fib Model Code*, respectively [26]. In Figure 8, f_t represents the tensile strength of PVA-ECC, and f_{Ftud} represents the residual tensile strength and is assumed to be $1/3$ f_t.

The calculation results are presented in Table 3. The mean value of P_{fib}/P_{Exp} is 0.84, with a coefficient of variation of 0.19. *fib Model Code* adopts the Prisco model [27] and the basic principles governing the structural design of fiber-reinforced concrete elements. Even though the contribution of fiber-reinforced concrete in tension is considered, the calculated load is still lower than the experimental value, but it is higher than the value calculated using GB 50010-2010 and ACI 318-19 for conventional concrete.

3.3. *Fehling*

Fehling [28] extended the design principles for ultra-high-performance concrete by taking fibers into consideration. In the design method, the plane-section assumption is used to define the strain profile, and the stress in the compression and tension zones is calculated from the corresponding constitutive models. However, the tensile stress of ultra-high-performance concrete is assumed to be uniformly distributed in the tension zone, which is different from the actual distribution of tensile stresses across a beam section. The stress–strain curve of ultra-high-performance concrete is defined by a stress–crack-width

relationship. Figure 9a shows the stress distributions and internal forces acting on the cross-section. The concrete compressive stresses are simplified as a triangle and the resulting stress F_{cd} lies at the centroid of the triangle. The distribution of tensile stresses is parabolic, which is directly in accordance with the minimum crack width. In this section, σ_{cf0d} is assumed to be f_t, as shown in Figure 9a. To simplify the calculation, the tensile stress distribution in Figure 9a can be converted to an equivalent stress block (see Figure 9b).

Table 3. Comparison of experimental ultimate load with values calculated using different codes and models.

Specimen	Experimental Results	GB 50010-2010 [24]		ACI 318-19 [25]		*Fib Model Code* [26]		UHPC [28]		Proposed Method [20]	
	Load (kN)	Load (kN)		Load (kN)		Load (kN)		Load (kN)			
	P_{Exp}	P_{GB}	P_{GB}/P_{Exp}	P_{ACI}	P_{ACI}/P_{Exp}	P_{fib}	P_{fib}/P_{Exp}	P_{UHPC}	P_{UHPC}/P_{Exp}	P_{Po}	P_{Po}/P_{Exp}
ECC-10-0.419	64.7	44.8	0.69	40.1	0.62	46.3	0.72	60.6	0.94	65.7	1.02
ECC-12-0.603	84.7	61.2	0.72	54.7	0.65	62.7	0.74	75.7	0.89	79.2	0.93
ECC-14-0.821	105.1	80.3	0.76	71.6	0.68	81.7	0.78	93.4	0.89	94.5	0.90
ECC-16-1.072	117.7	105.9	0.90	94.1	0.80	107.3	0.91	117.8	1.00	114.7	0.97
ECC-18-1.357	142.4	127.4	0.89	112.8	0.79	128.7	0.90	138.6	0.97	130.9	0.92
ECC-20-1.675	153.4	155.6	1.01	137.1	0.89	156.7	1.02	173.9	1.13	151.4	0.99
Mean value			0.83		0.74		0.85		0.97		0.95
Coefficient of variation			0.20		0.28		0.19		0.09		0.06

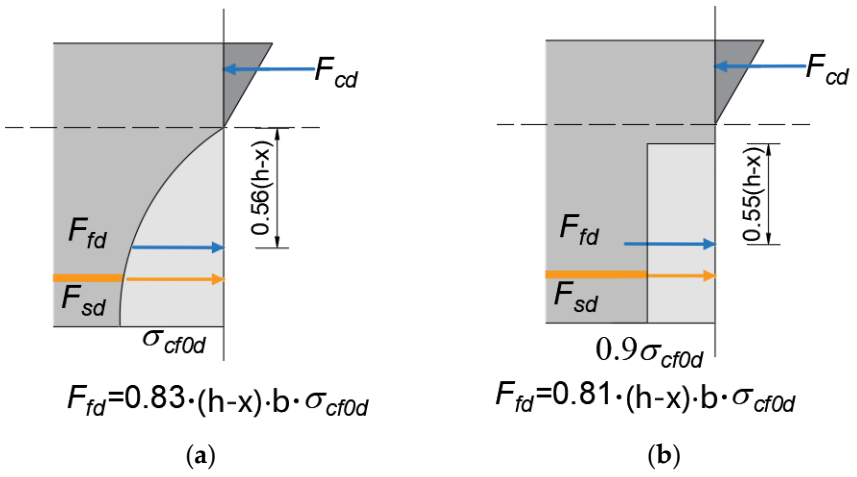

Figure 9. Assumed stress distribution and resultant tensile force at ultimate limit state: (**a**) realistic stress distribution; (**b**) simplified diagram.

Table 3 shows the comparison between the experimental result and that calculated by using the method proposed by Fehling. It can be observed that the mean load ratio is 0.97, with a coefficient of variation of 0.09. Thus, the calculated result is in good agreement with the experimental result. However, the tensile stress distribution in the tension zone is a bit different from that of ECC in tension and should be properly modified in the subsequent study.

4. Proposed Calculation Method

Wang et al. [20] suggested a calculation method to compute the moment capacity and peak load of singly reinforced PVA-ECC beams. The constitutive model of ECC in tension is modified in the design method, especially at the formation stage of microcracks, namely, the plateau stage of tensile stresses. Two limiting reinforcement ratios are developed based on different flexural behavior in Equations (4) and (5), namely, the minimum reinforcement ratio and the balanced reinforcement ratio. When the reinforcement ratio is lower than the

minimum reinforcement ratio, the failure mode of flexural beams is characterized by the fracture of reinforcement following the formation of a principle crack at the mid-span of beams. Once the reinforcement ratio is higher than the minimum reinforcement ratio, the failure mode changes from major cracking to crushing of PVA-ECC in the compression zone. The balanced reinforcement ratio represents the case in which the ultimate tensile strain of PVA-ECC in the tension zone and the ultimate compressive strain in the compression zone are achieved simultaneously.

$$\rho_{min} = \frac{0.16 f_t}{f_u - f_y} \tag{4}$$

$$\rho_t = \frac{\left[f_c'\left(0.75\varepsilon_{c,p} - 0.5\varepsilon_{c,1/2}\right) - f_t\left(\varepsilon_{t,p} - 0.5\varepsilon_{t,1}\right)\right]}{f_y\left(\varepsilon_{t,p} + \varepsilon_{c,p}\right)} \tag{5}$$

where ρ_{min} is the minimum reinforcement ratio and ρ_t is the balanced ratio.

With increasing reinforcement ratio, it is possible that the reinforcement does not yield when the ultimate compressive strain of PVA-ECC beams is obtained. Therefore, the yield reinforcement ratio when the yielding of tensile reinforcement and crushing of compressive PVA-ECC occur simultaneously is suggested in Equation (6).

$$\rho_y = \frac{\left[f_c'\left(0.75\varepsilon_{c,p} - 0.5\varepsilon_{c,1/2}\right)(h - a_s) - f_t\left(\varepsilon_y h + \varepsilon_{c,p} a_s - 0.5\varepsilon_{t,1}(h - a_s)\right)\right]}{f_y\left(\varepsilon_y + \varepsilon_{c,p}\right)h} \tag{6}$$

Based on different calculation equations of reinforcement ratio, all the values of ρ_{min}, ρ_t, and ρ_y for different rebar diameters are calculated and presented in Table 4.

Table 4. Minimum, balance, and yield reinforcement ratio for different steel diameters.

Diameter (mm)	Actual Reinforcement Ratio (%)	Minimum Reinforcement Ratio (%)	Balanced Reinforcement Ratio (%)	Yield Reinforcement Ratio (%)
10	0.419	0.297	0.390	1.806
12	0.603	0.201	0.407	1.772
14	0.821	0.199	0.416	1.903
16	1.072	0.202	0.405	1.741
18	1.357	0.183	0.419	1.945
20	1.675	0.200	0.414	1.911
Mean value		0.214	0.409	1.846

It can be seen from Table 4 that the minimum reinforcement ratio, balanced reinforcement ratio, and yield reinforcement ratio are close to each other for different rebar diameters. The average values for ρ_{min}, ρ_t, and ρ_y are 0.214%, 0.409%, and 1.846% for the HRB400-deformed steel bar, respectively. The actual reinforcement ratio in reference [21] was between the average balanced reinforcement ratio of 0.409% and the yield reinforcement ratio of 1.846%. Hence, the tensile reinforcement is in the post-yielded stage, while the compression strain at the edge of the compression zone reaches the peak compression strain when the beam is at the peak load.

A calculation method is also proposed to calculate the ultimate moment capacity of reinforced PVA-ECC beams in bending. Figure 10 shows the proposed method for the calculation of ultimate load, which is controlled by the crushing of PVA-ECC in the compression zone, namely, compression-control failure. Compared with the design method by Fehling [28] for ultra-high-performance concrete, the constitutive model in the tension and compression zone of beams is simplified bilinear, as shown in Figure 10. The plane-section assumption and force equilibrium are adopted in the calculation procedures.

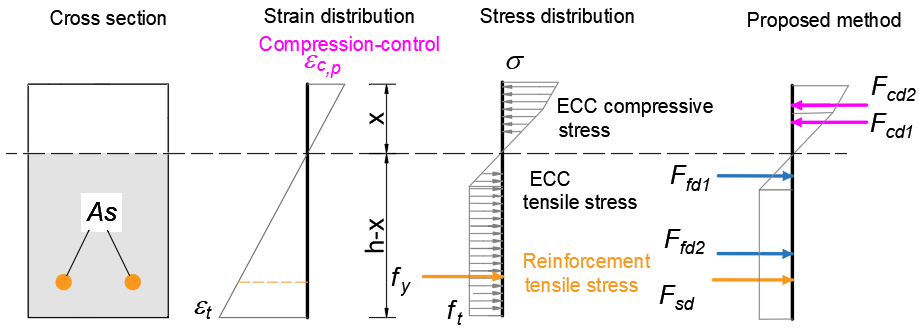

Figure 10. Proposed methods for calculation of ultimate load of beams in bending.

Table 3 lists the comparisons of the calculated load capacity and the experimental loads. The mean ratio and coefficient of variation of the calculated load capacity to the experimental loads are 0.95 and 0.06, respectively. Figure 11 shows the comparison among experimental results and calculated results based on different methods. It can be observed that the design methods in GB 50010-2010 [24], ACI 318-19 [25], and *fib Model Code* [26] significantly underestimate the ultimate load of reinforced PVA-ECC beams, as shown in Figure 11a, particularly when the diameter of longitudinal reinforcement is small, as the tensile strength of PVA-ECC is not considered in the design methods. When the bilinear constitutive model for PVA-ECC is considered in the numerical model and the proposed method, the ultimate load of beams can be predicted with good accuracy, as shown in Figure 11b.

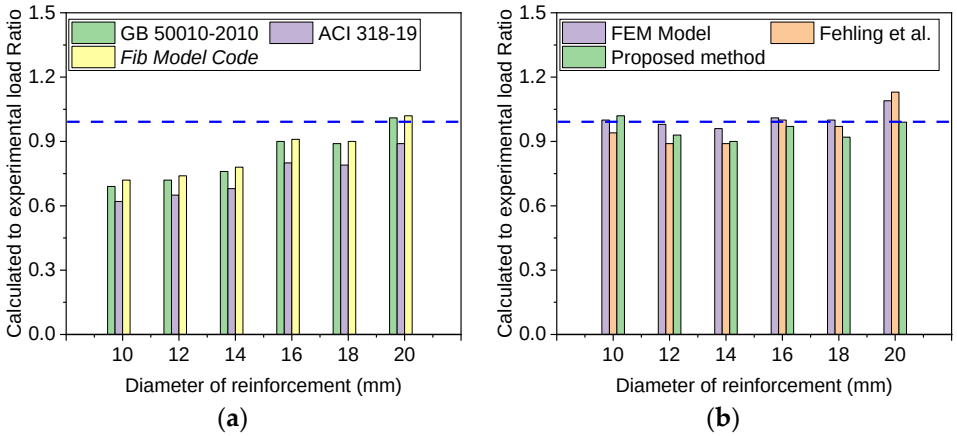

Figure 11. Ratio between analytical and experimental results with different calculation methods. (**a**) Results using design standards. (**b**) Results using FEM, Fehling et al., and proposed method.

5. Conclusions

In this study, a nonlinear finite element model is proposed for singly supported PVA-ECC beams in bending to simulate the load–deflection curve and failure mode. In the numerical model, the constitutive models for PVA-ECC are represented by simplified piece-wise linear curves, and the bond–slip behavior between the embedded reinforcing bar and surrounding PVA-ECC is considered in the numerical model. Calculation methods in different design codes are used to calculate the ultimate load of PVA-ECC beams. Moreover, a design method is also proposed to consider the tensile strength of PVA-ECC in calculation. The following conclusions can be obtained from the numerical study and design method.

(1) By considering the piece-wise constitutive models for PVA-ECC in tension and compression and the bond–slip behavior between PVA-ECC and steel reinforcement in the numerical model, the numerical results show a good agreement with the experiment results in terms of the load–deflection curves and failure modes. The ultimate load and deformation capacity of reinforced PVA-ECC beams can be predicted by using the numerical

model with good accuracy. The average numerical-to-experimental ratio of load capacities is 1.04, and the mean ratio of the numerical to experimental deflection at the fracture of reinforcement is 0.96.

(2) Parameter analyses show that increasing the reinforcement ratio of reinforced PVA-ECC beams significantly increases the stiffness after cracking and the ultimate load of beams. However, the increase in reinforcement strength grade has a limited effect on the initial stiffness of beams, whereas the ultimate load-bearing capacity of beams is effectively increased. The tensile localization strain of PVA-ECC affects the deformation capacity of beams. The deformation capacity of reinforced PVA-ECC beams is increased by increasing the tensile localization strain.

(2) The ultimate load of PVA-ECC beams is calculated using three different design codes, ACI 318-10, GB 50010-2010, and *fib Model Code*. All design methods underestimate the ultimate load of PVA-ECC beams due to the neglection of the tensile strength of PVA-ECC in the tension zone. By considering the tensile strength of PVA-ECC in the tension zone, the method proposed by Fehling can yield more accurate predictions of experimental results.

(3) When the tensile stress–strain relationship is considered, the proposed design method for reinforced PVA-ECC beams can predict the ultimate load of PVA-ECC beams accurately by dividing the failure modes into tension-control and compression control.

Author Contributions: Conceptualization, S.-B.K. and Q.-L.F.; methodology, D.-D.W.; software Q.-L.F.; validation, D.-D.W. and S.-B.K.; formal analysis, D.-D.W.; investigation, Q.-L.F.; writing—original draft preparation, Q.-L.F. and D.-D.W.; writing—review and editing, S.-B.K.; supervision, S.-B.K.; project administration, D.-D.W.; funding acquisition, Q.-L.F. All authors have read and agreed to the published version of the manuscript.

Funding: This research was funded by the Natural Science Foundation of Chongqing, China (Grant No. cstc2021jcyj-msxmX0357) and the Graduate Research and Innovation Foundation of Chongqing, China (Grant No. CYB21030), the Chongqing Commission of Education (Grant No.: KJQN202103802 and KJQN202103801), and the Chongqing Water Resources and Electric Engineering College (Grant No.: K202214).

Institutional Review Board Statement: Not applicable.

Informed Consent Statement: Not applicable.

Data Availability Statement: The data presented in this study are available on request from the corresponding author.

Conflicts of Interest: The authors declare no conflict of interest.

Notation

a_s	thickness of the concrete cover	P_{ACI}	peak load calculated by ACI 318-19
A_s	cross-sectional area of reinforcement	P_{Exp}	peak load of experimental results
b	width of cross-section	P_{FE}	peak load of numerical results
d	diameter of reinforcement	P_{fib}	peak load calculated by *fib Model Code*
D_{Exp}	experimental deflection at ultimate load	P_{GB}	peak load calculated by GB 50010-2010
D_{FE}	numerical deflection at ultimate load	P_{P_0}	peak load calculated by proposed method
E_c	elastic modulus of ECC	P_{UHPC}	peak load calculated by Fehling's method
E_h	hardening modulus of steel bars	s_1	slip at peak bond stress
E_s	elastic modulus of steel bars	s_2	slip at the onset of frictional bond stress
f'_c	compressive strength	$\varepsilon_{c,1/2}$	compressive strain at 50% of peak strength
f_d	compressive stress in the compression zone that adopts the compressive strength	$\varepsilon_{c,p}$	compressive strain at compressive strength
f_{Ftud}	ultimate strength, assumed as $1/3f_t$	$\varepsilon_{c,u}$	compressive strain at 50% of compressive strength
f_t	tensile strength	$\varepsilon_{s,u}$	ultimate tensile stain of steel
$f_{t,cr}$	cracking tensile strength	$\varepsilon_{t,1}$	cracking strain of ECC
f_u	ultimate strength of reinforcement	$\varepsilon_{t,cr}$	tensile strain when the stress is 95% of peak stress
f_y	yield strength of reinforcement	$\varepsilon_{t,p}$	tensile localization strain

f_r	residual stress of PVA-ECC	$\varepsilon_{t,u}$	ultimate tensile strain of ECC
F_{cd}	force in the compression zone	ρ_{min}	minimum reinforcement ratio
F_{cd1}	force in the initial compression zone	ρ_t	balanced reinforcement ratio
F_{cd2}	force in the second compression zone	ρ_y	yield reinforcement ratio
F_{fd}	force of ECC in tension zone	β_b	simplified coefficient
F_{fd1}	force of increasing stage in tension zone	σ_{cf0d}	tensile stress at the bottom of the tension zone, assumed to be f_t
F_{fd2}	force of plateau stage in tension zone	τ_{max}	maximum bond stress
F_{sd}	reinforcement force	τ_f	frictional bond stress
M	moment of beams in bending	λ	a coefficient that adopts 0.8
h	height of cross-sections	η	a coefficient that adopts 1

References

1. Jin, H.; Li, F.; Hu, D. Research on the flexural performance of reinforced engineered cementitious composite beams. *Struct. Concr.* **2021**, *23*, 2198–2220.
2. Maalej, M.; Li, V.C. Introduction of Strain-Hardening Engineered Cemenetitious Composites in Design of Reinforced Concrete Flexural Members for Improved Durability. *ACI Struct. J.* **1995**, *92*, 167–176.
3. Yang, E.; Li, V.C. Strain-Hardening Fibre Cement Optimization and Component Tailoring by Means of a Micromechanical Model. *Constr. Build. Mater.* **2010**, *24*, 130–139.
4. Victor, C.L. *Engineered Cementitious Composites (ECC): Bendable Concrete for Sustainable and Resilient Infrastructure*; Springer: Berlin/Heidelberg, Germany, 2022.
5. Ge, W.; Ashour, A.F.; Cao, D.; Lu, W.; Gao, P.; Yu, J.; Ji, X.; Cai, C. Experimental study on flexural behavior of ECC-concrete composite beams reinforced with FRP bars. *Compos. Struct.* **2019**, *208*, 454–465.
6. Yuan, F.; Pan, J.; Leung, C.K.Y. Flexural Behaviors of ECC and Concrete/ECC Composite Beams Reinforced with Basalt Fiber-Reinforced Polymer. *J. Compos. Constr.* **2013**, *17*, 591–602.
7. Dabiri, H.; Kaviani, A.; Kheyroddin, A. Influence of reinforcement on the performance of non-seismically detailed RC beam-column joints. *J. Build. Eng.* **2020**, *31*, 101333.
8. Behnam, H.; Kuang, J.S.; Samali, B. Parametric finite element analysis of RC wide beam-column connections. *Comput. Struct.* **2018**, *205*, 28–44.
9. Onuralp, O.Y.; Karalar, M.; Aksoylu, C.; Beskopylny, A.N.; Stel, S.A.; Shcherban, E.M.; Qaidi, S.; Pereira, I.D.S.A.; Monteiro, S.N.; Azevedo, A.R.G. Shear performance of reinforced expansive concrete beams utilizing aluminium waste. *J. Mater. Res. Technol.* **2023**, *24*, 5433–5448.
10. Ozkılıç, Y.O.; Basaran, B.; Aksoylu, C.; Karalar, M.; Martins, C.H. Mechanical behavior in terms of shear and bending performance of reinforced concrete beam using waste fire clay as replacement of aggregate. *Case Stud. Constr. Mater.* **2023**, *18*, e02104.
11. Shao, Y.; Billington, S.L. Flexural performance of steel-reinforced engineered cementitious composites with different reinforcing ratios and steel types. *Constr. Build. Mater.* **2020**, *231*, 117159.
12. Shao, Y. *Improving Ductility and Design Methods of Reinforced High-Performance Fiber-Reinforced Cementitious Composite (HPFRCC) Flexural Members*; Stanford University: Stanford, CA, USA, 2020.
13. Shao, Y.; Billington, S.L. Predicting the two predominant flexural failure paths of longitudinally reinforced high-performance fiber-reinforced cementitious composite structural members. *Eng. Struct.* **2019**, *199*, 109581.
14. Suryanto, B.; Nagai, K.; Maekawa, K. Modeling and Analysis of Shear-Critical ECC Members with Anisotropic Stress and Strain Fields. *J. Adv. Concr. Technol.* **2010**, *8*, 239–258.
15. Suryanto, B.; Nagai, K.; Maekawa, K. Smeared-Crack Modeling of R/ECC Membranes Incorporating an Explicit Shear Transfer Model. *J. Adv. Concr. Technol.* **2010**, *8*, 315–326.
16. Varela, S.; Saiidi, M.S. *Shear Behavior of Engineered Cementitious Composite Structural Members, Second Conference on Smart Monitor, Assessment and Rehabilitation of Civil Structures*; ITU: Istanbul, Turkey, 2013.
17. Zheng, Y.-Z.; Wang, W.-W.; Mosalam, K.M.; Fang, Q.; Chen, L.; Zhu, Z.-F. Experimental investigation and numerical analysis of RC beams shear strengthened with FRP/ECC composite layer. *Compos. Struct.* **2020**, *246*, 112436.
18. Shanour, A.S.; Said, M.; Arafa, A.I.; Maher, A. Flexural performance of concrete beams containing engineered cementitious composites. *Constr. Build. Mater.* **2018**, *180*, 23–34.
19. Selim, A.H.; Mahmoudi, F.; Abdalla, J.A.; Hawileh, R.A.; Abed, F.; Kyaure, M. Finite Element Modeling of Engineered Cementitious Composite (ECC) Prisms and Beams. In Proceedings of the 2022 Advances in Science and Engineering Technology International Conferences (ASET), Dubai, United Arab Emirates, 21–24 February 2022; IEEE: Piscataway, NJ, USA; pp. 1–6.
20. Shao, Y.; Hung, C.-C.; Billington, S.L. Gradual Crushing of Steel Reinforced HPFRCC Beams: Experiments and Simulations. *J. Struct. Eng.* **2021**, *147*, 04021114.
21. Wang, D.-D.; Li, J.-Z.; Qin, S.-D.; Liu, C.-X.; Long, B.; Kang, S.-B. Experimental tests and analytical model for reinforced polyvinyl alcohol-engineered cementitious composite beams in bending. *Struct. Concr.* **2023**, *24*, 3520–3544.
22. DIANA. DIANA Users' Manual Release 10.2, DIANA FEA bv. 2017. Available online: https://manuals.dianafea.com/d102/Diana.html (accessed on 21 June 2023).
23. Bandelt, M.J.; Frank, T.E.; Lepech, M.D.; Billington, S.L. Bond behavior and interface modeling of reinforced high-performance fiber-reinforced cementitious composites. *Cem. Concr. Compos.* **2017**, *83*, 188–201.

24. 50010–2010; Code for Design of Concrete Structures. National Standard of The People's Republic Of China: Beijing, China, 2015.
25. ACI 318–19; Building Code Requirements for Structural Concrete. Americon Concrete Institute: Farming, MI, USA, 2019.
26. *fib Model Code for Concrete Structures 2010*; Fédération Internationale du Béton: Laussane, Switzerland, 2013.
27. Prisco, M.D.; Colombo, M.; Dozio, D. Fibre-reinforced concrete in fib Model Code 2010: Principles, models and test validation. *Struct. Concr.* **2013**, *14*, 342–356.
28. Fehling, E.; Schmidt, M.; Walraven, J.; Leutbecher, T.; Frohlich, S. *Ultra-High Performance Concrete UHPC: Fundamentals, Design, Examples*; Ernst & Sohn GmbH & Co.: Berlin/Heidelberg, Germany, 2014.